Research Article | Vol. 31, No. 7 / 27 Mar 2023 / Optics Express 11213

Optics EXPRESS

# Assessment of lateral resolution of single random phase encoded lensless imaging systems

SAURABH GOSWAMI, PRANAV WANI, GAURAV GUPTA, AND BAHRAM JAVIDI*

*Electrical Engineering Department, University of Connecticut, 371 Fairfield Road, Unit 2157 Storrs, CT 06269, USA*
*bahram.javidi@uconn.edu*

**Abstract:** In this paper, we have used the angular spectrum propagation method and numerical simulations of a single random phase encoding (SRPE) based lensless imaging system, with the goal of quantifying the spatial resolution of the system and assessing its dependence on the physical parameters of the system. Our compact SRPE imaging system consists of a laser diode that illuminates a sample placed on a microscope glass slide, a diffuser that spatially modulates the optical field transmitting through the input object, and an image sensor that captures the intensity of the modulated field. We have considered two-point source apertures as the input object and analyzed the propagated optical field captured by the image sensor. The captured output intensity patterns acquired at each lateral separation between the input point sources were analyzed using a correlation between the captured output pattern for the overlapping point-sources, and the captured output intensity for the separated point sources. The lateral resolution of the system was calculated by finding the lateral separation values of the point sources for which the correlation falls below a threshold value of 35% which is a value chosen in accordance with the Abbe diffraction limit of an equivalent lens-based system. A direct comparison between the SRPE lensless imaging system and an equivalent lens-based imaging system with similar system parameters shows that despite being lensless, the performance of the SRPE system does not suffer as compared to lens-based imaging systems in terms of lateral resolution. We have also investigated how this resolution is affected as the parameters of the lensless imaging system are varied. The results show that SRPE lensless imaging system shows robustness to object to diffuser-to-sensor distance, pixel size of the image sensor, and the number of pixels of the image sensor. To the best of our knowledge, this is the first work to investigate a lensless imaging system's lateral resolution, robustness to multiple physical parameters of the system, and comparison to lens-based imaging systems.



## 1. Introduction

Conventional imaging systems use lenses which may make them bulky and costly. Removal of lenses and/or incorporating random phase modulations may greatly improve the compactness of imaging systems [1–7]. Lensless imaging, as a compact and less expensive alternative to lens-based imaging, has become an attractive field of research recently. In the lensless imaging system investigated here [1,2], the main optical elements are diffusers that cause the light passing through an object to be randomly phase modulated and then captured on an image sensor. Such systems with a single diffuser are referred to as single random phase encoding (SRPE) [1] systems here. Removal of microscope objective lenses in digital holography may alleviate the spatial-frequency bandwidth restriction imposed by the numerical aperture (NA) of lenses and improve field-of-view [4]. Images obtained from SRPE systems can be directly used and without computational reconstruction with convolutional neural networks (CNN) for tasks such

#480591 https://doi.org/10.1364/OE.480591
Journal © 2023 Received 10 Nov 2022; revised 7 Feb 2023; accepted 8 Feb 2023; published 17 Mar 2023

Optics EXPRESS

as classification [5]. Recent studies have shown that these systems are capable of capturing and reconstructing 3D information of an object [6]. Importantly, the accuracy of deep neural network-assisted classification of SRPE systems remains virtually unaffected even when the number of image sensor pixels is drastically reduced [7]. An imaging device with such attractive properties should be thoroughly analyzed at a system level. Even though previous works have experimentally investigated the various properties of SRPE systems such as robustness to sensor pixel counts [7], and noise-robustness [5], it is beneficial to investigate the connection between these properties and the physical parameters of the imaging system.

Our SRPE imaging system [5,7] is compact and field portable. It consists of a laser diode that emanates a partially coherent optical field, a microscope glass slide at the object plane on which the sample under the observation is placed, a diffuser that spatially phase-modulates the field transmitting through the object, and an image sensor that captures the intensity of the modulated field. Figure 1 shows a schematic diagram of this system.

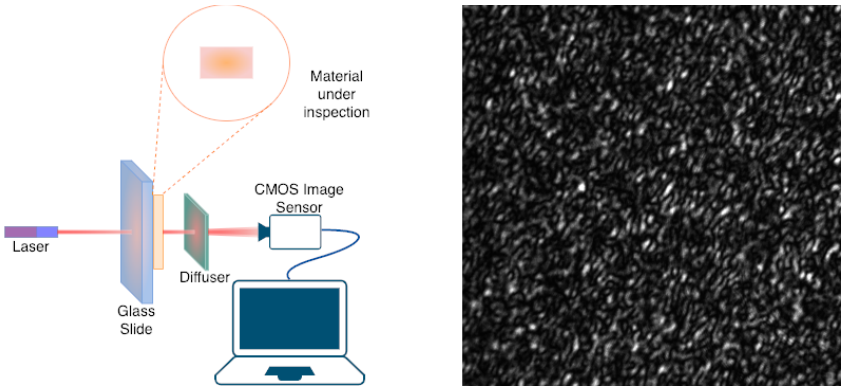


**Fig. 1.** A schematic diagram of the SRPE imaging system (left) and, a sample intensity pattern captured by the image sensor.

Lateral resolution is a parameter of primary interest for any imaging system [8]. For conventional lens-based imaging systems, the lateral resolution may be defined using well-defined point spread function. However, the intensity captured by the camera in a lensless SRPE system is pseudorandom patterns spread over the entire image sensor and hence are incompatible with visual resolution criteria such as Rayleigh criterion [9], or Sparrow's criterion [10]. In this paper, we present an investigation into the lateral resolution of lensless SRPE imaging systems, its dependence on the physical parameters of the imaging system, and robustness to several important system parameters such as pixel-size of the image sensor, the number of sensor-pixels, and system size.

For analysis of the lateral resolution, we considered two-point source apertures in the object plane of the proposed SRPE imaging system. The light propagated by the two point sources is scattered by the diffuser and captured at the image sensor plane of the SRPE system which was then analyzed. Using angular spectrum propagation, we propagated the optical field from the two-point source apertures through the diffuser and then to the image sensor. Given that the propagation distances of the field are either smaller or comparable to the dimension of the optical elements, a paraxial approximation would not be accurate, thus making the use of angular spectrum propagation indispensable. However, since angular spectrum propagation does not give us closed-form theoretical expressions, we have used numerical simulations to finalize our analyses. To calculate the estimate of the lateral resolution of our lensless SRPE imaging system, we have used the following approach. We considered two-point source-apertures as the input object and obtained the propagated optical field captured by the image sensor. Initially, the

Optics EXPRESS

two point-sources are overlapping. Then, we gradually increased the separation between the two point-sources from 0 to a few microns and obtained their corresponding intensity pattern, as sampled by a pixelated camera. The captured output intensity patterns acquired at each lateral separation between the input point sources were analyzed using a correlation between the captured output pattern for the original overlapping two point-sources, and the captured output intensity for the separated point sources. The correlation between the captured output intensity corresponding to two overlapping point-sources and the captured output intensity due to separated point-sources is a monotonically decreasing function of the point sources separation. The lateral separation for which this correlation fell below a threshold value of 35% of the maximum value has been defined as the resolution of this system. The 35% threshold corresponds to the Abbe diffraction limit of an equivalent lens-based imaging system. Under this same definition, we also calculated the lateral resolution of an equivalent lens-based imaging system that has similar system parameters to the lensless SRPE system. We show that the lensless SRPE competes well with lens-based imaging even for high numerical aperture lenses. Our analysis relates the lateral resolution to the design parameters of the SRPE imaging system and hence provides a guideline to optimize SRPE imaging systems for specific applications.

The rest of this paper is organized as follows. In section 2, we briefly describe the propagation phenomenon inside the SRPE imaging system and our approach to the resolution analysis. In section 3, we use the expressions specified in section 2 to obtain the lateral resolution limit of the SRPE lensless imaging system, compare it with an equivalent lens-based imaging system and assess its dependence on the physical parameters of the imaging system. Section 4 presents the Conclusion. Appendix A provides a table with the list and definition of the various parameters used in the manuscript.

## 2. Methodology

### 2.1. Lensless imaging with single random phase encoding

Lensless SRPE imaging systems are a class of computational imaging systems that may rely on statistical [1] or machine learning algorithms to make use of the information in the captured intensity pattern. Unlike conventional lens-based imaging systems, lensless SRPE systems may distribute the modulated input information over the entire image sensor plane (see Fig. 1). This causes the captured intensities when processed statistically or by CNNs to perform classification, even using only a small subset of the sensor pixel intensities [7]. Figure 2 shows a lensless SRPE system that was developed in our lab and Fig. 3 shows a comparison between intensities acquired with a lens-based imaging system and a lensless SRPE imaging system. As shown in Fig. 2, the lensless SRPE imaging system can be a compact 3D printed unit. In our experiments, the system has dimensions $58mm \times 85mm \times 118.5mm$ that house all the components, i.e., the laser diode, the glass slide, the diffuser, and the camera. Our system has the same configuration as proposed in [5,7].

Figure 1 shows a schematic diagram of the system and Fig. 4 illustrates the field propagation from light source to the image sensor. In [7], the compact 3D-printed setup was used to perform automated disease identification using red blood cells. In this work, we consider this optical system to investigate its physical properties.

We denote the coordinates of the object plane as $(x, y)$, the diffuser plane as $(\zeta, \eta)$, and the CMOS image sensor plane as $(\alpha, \beta)$. Since the goal of the analysis is to calculate the spatial resolution of the system, we have started with the conventional idea of considering two-point source-apertures separated by a known distance in the object plane. One point-source is at the origin and the other is located at $x_0$ away on the x-axis (Fig. 4).

For two-point source-apertures, the field $u_0(x, y)$ transmitting through the object plane becomes:

$$u_0(x, y) = \delta(x, y) + \delta(x - x_0, y) \tag{1}$$

Optics EXPRESS

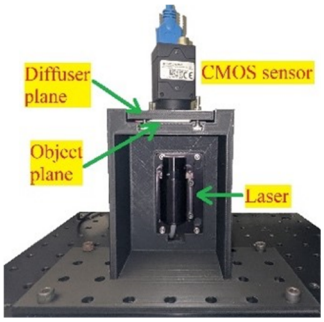


**Fig. 2.** Compact 3D printed SRPE system with dimensions $58mm \times 85mm \times 118.5mm$.

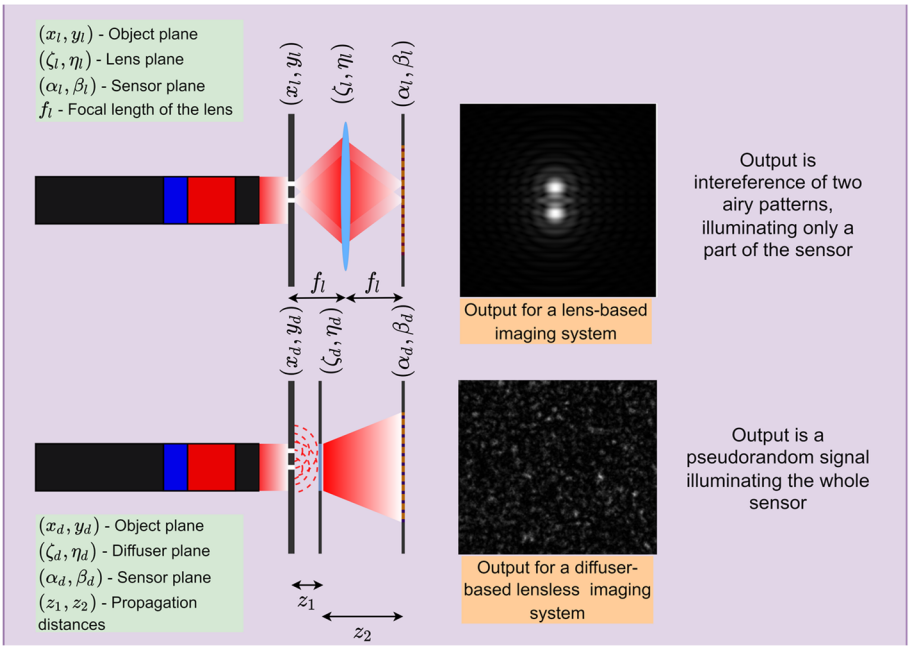


**Fig. 3.** Comparison of lens-based (top) imaging and lensless SRPE imaging (bottom) systems.

Optics EXPRESS

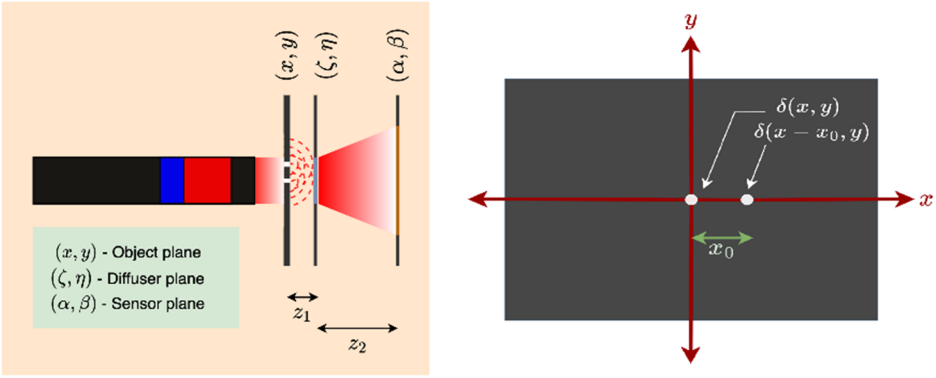


**Fig. 4.** Propagation of light due to two point-apertures at the object plane (left) to the output (image sensor), and placement of the point sources on the object plane (right).

The Fourier transform of point sources contains all possible spatial frequencies. However, due to the finite dimension $(D_\zeta, D_\eta)$ of the rectangular diffuser, as shown in Fig. 5, the maximum frequency $(f_{xm}, f_{ym})$ collected by the diffuser would be:

$$f_{xm} = \frac{1}{\lambda}\cos\theta_{xm} = \frac{\frac{D_\zeta}{2}}{\lambda\sqrt{z_1^2 + \frac{D_\zeta^2}{4}}}, \; f_{ym} = \frac{1}{\lambda}\cos\theta_{ym} = \frac{\frac{D_\eta}{2}}{\lambda\sqrt{z_1^2 + \frac{D_\eta^2}{4}}} \tag{2}$$

where $\theta_{xm}$ and $\theta_{ym}$ are the angles of the marginal rays of the diffuser measured with respect to the $x$ and the $y$-axis. This can be achieved by low pass filtering the incoming field with cut-off frequency $(f_{xm}, f_{ym})$:

$$\overline{u_0(x,y)} = u_0(x,y) * h_D(x,y) \tag{3}$$

Here $*$ denotes convolution and $h_D(x,y)$ is an ideal low-pass filter defined with impulse response:

$$h_D(x,y) = f_{xm} f_{ym} Sinc(x f_{xm}) Sinc(y f_y) \tag{4}$$

After propagating a small distance $z_1$ to the diffuser, the field using angular spectrum propagation [11] becomes:

$$u_1(\zeta,\eta) = \overline{u_0(\zeta,\eta)} * \mathcal{F}^{-1}\left[\exp\left(\frac{j2\pi z_1}{\lambda}\sqrt{1 - \lambda^2 f_x^2 - \lambda^2 f_y^2}\right)\right] \tag{5}$$

where $\mathcal{F}^{-1}[\cdot]$ denotes inverse Fourier transform and $(f_x, f_y)$ denote the spatial frequencies corresponding to the $(x,y)$ plane. The incoming field is modulated by diffuser transmittance function $t_D(\zeta,\eta)$ defined as follows

$$t_D(\zeta,\eta) = \exp(j\phi(\zeta,\eta)) Rect\left(\frac{\zeta}{D_\zeta}, \frac{\eta}{D_\eta}\right) \tag{6}$$

where $\phi(\zeta,\eta)$ is a random phase angle uniformly distributed between $[-\pi, \pi]$. This is an established mathematical model for thin diffusers that was also used in previous works such as [5]. Even though more advanced models are available, this model is the simplest. The modulated signal can be expressed as follows:

$$u_1'(\zeta,\eta) = t_D(\zeta,\eta) u_1(\zeta,\eta) \tag{7}$$

The modulated field leaving the diffuser further propagates a distance $z_2$ to reach the image sensor. Since the image sensor also has a finite aperture $(S_\alpha, S_\beta)$, it would also limit the frequency

Optics EXPRESS

content of the incoming field. The limiting frequencies ($f_{\zeta m}$,$f_{\eta m}$) corresponding to the sensor can be given as

$$f_{\zeta m} = \frac{1}{\lambda}\cos\theta_{\zeta m} = \frac{S_\alpha/2}{\lambda\sqrt{z_2^2 + \frac{S_\alpha^2}{4}}},\ f_{\eta m} = \frac{1}{\lambda}\cos\theta_{\eta m} = \frac{S_\beta/2}{\lambda\sqrt{z_2^2 + \frac{S_\beta^2}{4}}} \tag{8}$$

where ($\theta_{\zeta m}, \theta_{\eta m}$) are the angles of the marginal rays of the sensor measured with respect to the $\zeta$ and $\eta$-axes. This is also equivalent to low-pass filtering the field emerging from the diffuser with cut-off frequency ($f_{\zeta m}$,$f_{\eta m}$):

$$\overline{u_2(\zeta,\eta)} = u_1^{'}(\zeta,\eta) * h_S(\zeta,\eta) \tag{9}$$

Here, $h_S(\zeta,\eta)$ is the impulse response of a low-pass filter defined as:

$$h_S(\zeta,\eta) = f_{\zeta m} f_{\eta m} Sinc(\zeta f_{\zeta m}) Sinc(\eta f_{\eta m}) \tag{10}$$

After propagating a distance $z_2$ to the sensor, the field becomes

$$u_2(\alpha,\beta) = Rect\left(\frac{\alpha}{S_\alpha}, \frac{\beta}{S_\beta}\right)\left[\overline{u_2(\alpha,\beta)} * \mathcal{F}^{-1}\left[\exp\left(\frac{j2\pi z_2}{\lambda}\sqrt{1-\lambda^2 f_\alpha^2 - \lambda^2 f_\beta^2}\right)\right]\right] \tag{11}$$

The image sensor records the intensity $i(\alpha,\beta)$ of the incident field

$$i(\alpha,\beta) = |u_2(\alpha,\beta)|^2 \tag{12}$$

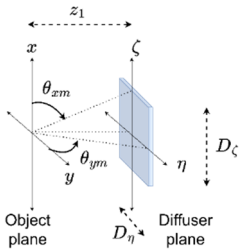


**Fig. 5.** Angles of the marginal rays for the diffuser with respect to the $x$ and $y$-axis.

### 2.2. Sampling with pixelated camera

The spatially continuous field incident on the CMOS image sensor is sampled at pixels of size ($p_\alpha, p_\beta$) centered at discrete locations ($m \times pix_\alpha, n \times pix_\beta$) where $(m,n)$ are pixel indices such that $-M/2 \le m \le M/2, -N/2 \le n \le N/2$ and, ($pix_\alpha, pix_\beta$) are pixel pitches along the $(\alpha,\beta)$ axes. The pixel intensity sampled at each of these locations is the average of the continuous intensity $i(\alpha,\beta)$ of all areas on the pixels. We denote this sampled intensity as $i_S[m,n]$ where $(m,n)$ are pixel indices:

$$i_S[m,n] = \frac{1}{P_A}\iint_{-\infty}^{\infty} i(\alpha,\beta) S(\alpha,\beta,p_\alpha,p_\beta,pix_\alpha,pix_\beta,M,N,m,n)\, d\alpha\, d\beta \tag{13}$$

In Eq. (13), $S(\alpha,\beta,p_\alpha,p_\beta,pix_\alpha,pix_\beta,M,N,m,n)$ or $S(\cdot)$ is the sampling function and $P_A$ is defined as:

$$P_A = \iint_{-\infty}^{\infty} S(\cdot)\, d\alpha\, d\beta \tag{14}$$

For our analysis, we used a rectangular sampling function, i.e.,

$$S(\cdot) = Rect\left(\frac{\alpha - m \times pix_\alpha}{p_\alpha}\right) Rect\left(\frac{\beta - n \times pix_\beta}{p_\beta}\right) Rect\left(\frac{m}{M}\right) Rect\left(\frac{n}{N}\right) \tag{15}$$

Optics EXPRESS

### 2.3. Analyzing lateral resolution using numerical simulation

To analyze the lateral resolution of the system, we have considered $\bar{N}$ different values of the source-separation $x_0$ (see Eq. (1)) starting from 0 to a maximum value of $x_{0\bar{N}}$ microns. The $j$-th such value would henceforth be denoted as $x_{0j}$. Hence, $x_{00} = 0$ micron represents two overlapping point sources. For each $x_{0j}$, we have calculated the acquired captured intensity pattern $i_{Sj}$ using Eq. (1)–(15). We define lateral resolution as the value $x_{0j*}$ at which the correlation $Corr(i_{S0}, i_{Sj})$ between $i_{S0}$ (for overlapping point-sources) and $i_{Sj*}$ (for separated point-sources) drops below a threshold value $th_{Corr}$. We use the Frobenius inner product between two sampled intensity patterns as the measure of correlation, i.e.,

$$Corr(i_{S0}, i_{Sj}) = \langle i_{S0}, i_{Sj} \rangle_{\mathbb{F}} \tag{16}$$

Given that correlation is a monotonically decreasing function of $x_0$, we use the threshold:

$$th_{Corr} = 0.35 \times Corr(i_{S0}, i_{S0}) \tag{17}$$

The value 0.35 was selected because the Abbe diffraction limit corresponds to ~35% correlation for an equivalent lens-based imaging system. The simulated estimate of lateral resolution of the single random phase encoding lensless imaging system would hence be:

$$x_{0j*} = \min_j(x_{0j}) \; such \; that \;\; Corr(i_{S0}, i_{Sj}) \leq th_{Corr} \tag{18}$$

## 3. Results

Given the point spread function obtained using the angular spectrum propagation and given that paraxial approximation would not be accurate for this scenario, it is difficult to analytically determine the spatial resolution of the single random phase encoding imaging systems. Hence, we assess the lateral resolution and its dependence on various physical parameters of the system using simulations. As our initial parameters, we have considered a wavelength $\lambda = 600$ nanometers, an object to diffuser distance $z_1 = 3.6$ millimeters, a diffuser to image-sensor distance $z_2 = 26.7$ millimeters, sensor pixel-size $p_\alpha = p_\beta = 0.6$ microns, diffuser-size $D_\zeta = D_\eta = 7.5$ millimeters and, sensor-size $S_\alpha = S_\beta = 7.5$ millimeters. During the simulations, both the diffuser plane and the image-sensor plane were laterally sampled at the rate of (0.60 microns, 0.60 microns). For all the simulations, we have varied one of the system parameters and kept all the others constant at the abovementioned values.

### 3.1. Estimate of lateral resolution

Our resolution analysis is inspired by the visual resolution criterion of lens-based imaging systems. In typical lens-based imaging systems, two point-sources placed at a certain distance apart on the object-plane create two airy patterns on the image sensor plane. Visual resolution criteria such as the Rayleigh criterion [9] are estimates of how close these point sources could be placed so that an observer can visually distinguish the central maxima of the two airy patterns on the image plane. Lensless imaging systems do not produce human-interpretable images. Hence, instead of visual cues, we rely on correlation (as defined in Eq. (16)) to identify when the acquired intensity pattern for two point-sources begins to be sufficiently different from the pattern corresponding to two overlapping point-sources. For the parameters mentioned above, we obtain the plot shown in Fig. 6. It shows that the correlation $Corr(i_{S0}, i_{Sj})$ drops below the threshold $th_{Corr}$ (i.e., 35% of $Corr(i_{S0}, i_{S0})$ at source-separation $x_{0j*} = 0.440$ microns. Hence, according to the definition in Eq. (18), this is the resolution of the SRPE lensless system with the initial system parameters.

Note that the resolution estimate obtained here is smaller than the sensor pixel size. In section 3.3, we show that this resolution estimate remains robust to a large range of sensor pixel sizes as well.

Optics EXPRESS

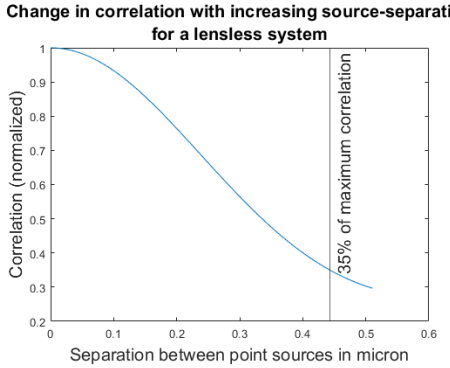


**Fig. 6.** Lateral resolution of lensless SRPE system estimated by change in correlation as a function of separation between two point-sources (Fig. 4) for initial parameters of simulation.

### 3.2. *Comparison of lateral resolution between a lens-based and lensless imaging system*

In this subsection, we have compared the simulated resolution estimate of the SRPE lensless imaging system (with the aforementioned parameters) with that of an equivalent lens-based imaging system. In this system, the diffuser was replaced with a lens while the propagation distances were kept the same as in the lensless imaging system. The configuration of this simulated lens-based imaging system is given in Fig. 7.

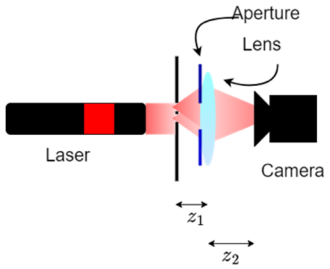


**Fig. 7.** The configuration of a lens-based imaging system with equivalent system parameters as the lensless imaging system. That is, $z_1$ and $z_2$ are the same as in lensless SRPE in Fig. 4, and the lens aperture is equal to the diffuser size.

To ensure that both the lens and the diffuser capture the same frequency content, we have simulated a thin aperture (with the same dimensions as the diffuser size) placed in-front of the lens. Also, to ensure that the lens produces a focused image of the object on the image sensor, we have kept the focal length $f_l$ as:

$$f_l = \frac{z_1 z_2}{z_1 + z_2} \tag{19}$$

To estimate the resolution for a lens based imaging, we used the same system parameters $z_1$, $z_2$, and diffuser size in the SRPE lensless imaging system in Fig. 4 to set up the lens based imaging. We set the lens diameter in Fig. 7 to be equal to the diffuser size in Fig. 4. For the initial system parameters (see Table 1), we found that the resolution estimate, as defined in Eq. (18), for the equivalent lens-based imaging system is 0.4 microns (see Fig. 8), which is 5.7% lower than the resolution estimate of the SRPE lensless imaging system with the same system parameters. This equivalent lens-based system has a numerical aperture (NA) of 1.16.

Optics EXPRESS

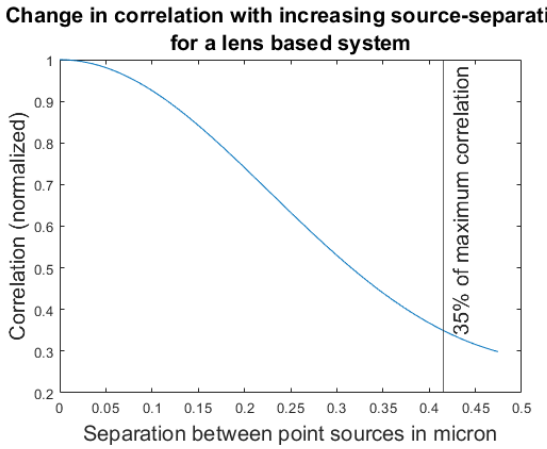


**Fig. 8.** Lateral resolution estimated by the change in correlation (Eq. (16)) as a function of separation between two ideal point-sources for a lens-based imaging system. The lens-based system has equivalent system parameters $z_1$ and $z_2$ (see Fig. 7) as the lensless SRPE system (see Fig. 4), and lens diameter equals to diffuser size. The numerical aperture of lens-based imaging system is 1.16. See Table 1 for additional details.

**Table 1. Resolution comparison of lens-based and lensless SRPE systems for different numerical apertures of lens-based imaging. For each comparison of resolution, the lens based imaging and lensless SRPE systems have the same physical parameters $z_1$ and $z_2$ (see Figs. 4 and 7). Also, the lens diameter equals to diffuser size. SRPE: Single Random Phase Encoding.**

| Numerical aperture of the equivalent lens-based imaging system | Lens-based imaging system | | | Corresponding lensless SRPE system | |
|---|---|---|---|---|---|
| | Lens-aperture (millimeters) | Focal length (millimeters) | Resolution (microns) | Diffuser-aperture (millimeters) | Resolution (microns) |
| 1.16 | 7.5 | 3.1 | 0.4 | 7.5 | 0.4 |
| 0.4 | 2.6 | 3.1 | 1.3 | 2.6 | 1.4 |
| 0.25 | 1.6 | 3.1 | 2.2 | 1.6 | 2.4 |

The numerical aperture of lenses used in typical optical systems may be smaller than 1.1. Thus, we have also calculated (using simulation) the resolution of lens-based imaging systems with numerical aperture values of 0.25 and 0.4 and compared the resolution to that of the lensless SRPE system with similar system parameters. To simulate these varying numerical apertures, we kept the focal length of the lens constant but reduced the aperture size of the lens (as shown in Table 1). The propagation distance between the object and the lens for a lens based system ($z_1$ in Fig. 7) or between the object and diffuser ($z_1$ in Fig. 4) for the lensless SRPE system were kept fixed at 3.6 millimeters. Likewise, the distance between the lens and the image-sensor for a lens based system ($z_2$ in Fig. 7) and the diffuser and image sensor ($z_2$ in Fig. 4) for the lensless SRPE system were kept fixed at 26.7 millimeters, i.e., the same as their aforementioned initial values. For a lens with a numerical aperture of 0.4, the resolution calculated using Eqs. (16)–(18) turned out to be 1.3 microns, which is 9% smaller than the resolution of the corresponding lensless SRPE system. For a lens with a numerical aperture of 0.25, the resolution was calculated to be 2.2 microns, which is 8% smaller than the resolution of the corresponding lensless SRPE system (see Table 1). These results show that lensless SRPE systems with a diffuser can provide resolution that competes well with commercially available lenses, even for high numerical aperture lenses.

Optics EXPRESS

### 3.3. *Effect of the physical parameters of the lensless imaging system on the lateral resolution*

In this section, we assess how different parameters of the lensless SRPE imaging system impact its lateral resolution (see Fig. 9,10). The lateral resolution of imaging systems usually decreases with increasing wavelength. The lensless SRPE imaging system under study exhibits the same property. Keeping all the other system parameters fixed at their initial values, we changed the wavelength of the illuminating light from 500 nanometers to 900 nanometers in steps of 40 nanometers. As shown in Fig. 9(a), this caused the spatial resolution to change from 0.354 microns to 0.653 microns. In this range of wavelength, the wavelength seems to affect the SRPE resolution in a linear fashion.

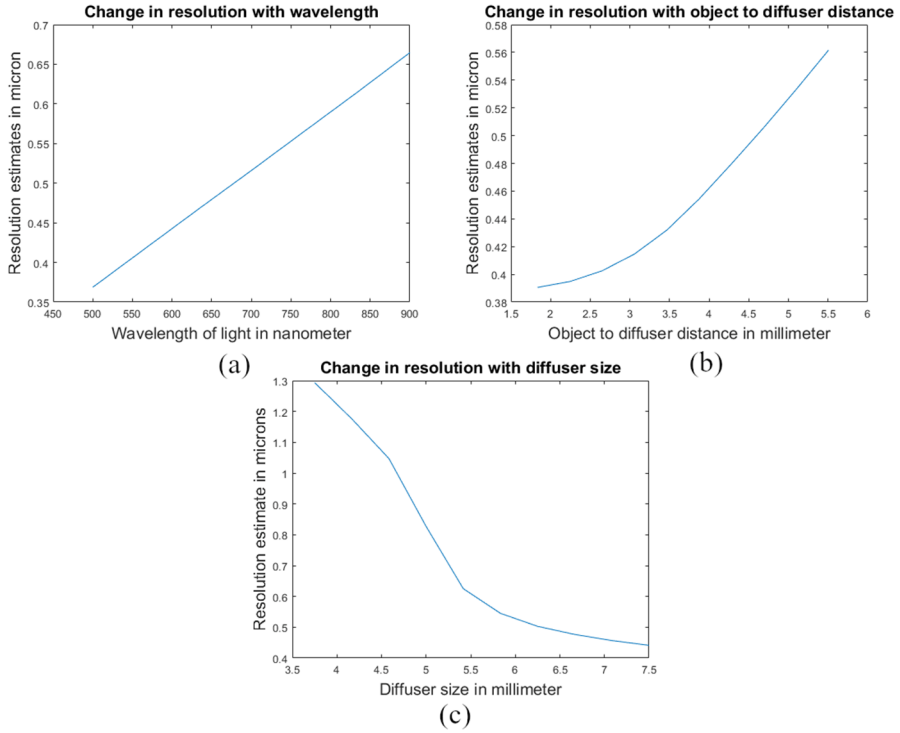


**Fig. 9.** Resolution estimate of the lensless SRPE system (see Fig. 4) as a function of (a) wavelength of the illuminating light, (b) distance between the object and the diffuser, and (c) size of the diffuser.

To assess the effect of the object to diffuser distance $z_1$ on the resolution estimate, we varied the distance between the object plane and the diffuser plane from 2.9 millimeters to 5.6 millimeters and kept all other parameters constant at their initial value. This caused the resolution estimate to increase from 0.390 microns to 0.564 microns (see Fig. 9(b)). This is expected as an increase in the object to diffuser distance $z_1$ causes a decrease in the maximum frequency $(f_{xm}, f_{ym})$ (see Eq. (2)) collected by the diffuser. A closer look at Fig. 9(b) shows that the relation between $z_1$ and resolution estimate is non-linear in this range of $z_1$.

As shown in Eq. (2), increasing the diffuser size increases the maximum frequency $(f_{xm}, f_{ym})$ that the diffuser can collect, resulting in an improvement in the resolution estimate. Figure 9(c) confirms this by showing that as we increase the diffuser size from 3.7 millimeters to 7.5 millimeters, the resolution estimate drops from 1.298 microns to 0.44 microns. All the other parameters were kept fixed at their initial values.

Optics EXPRESS

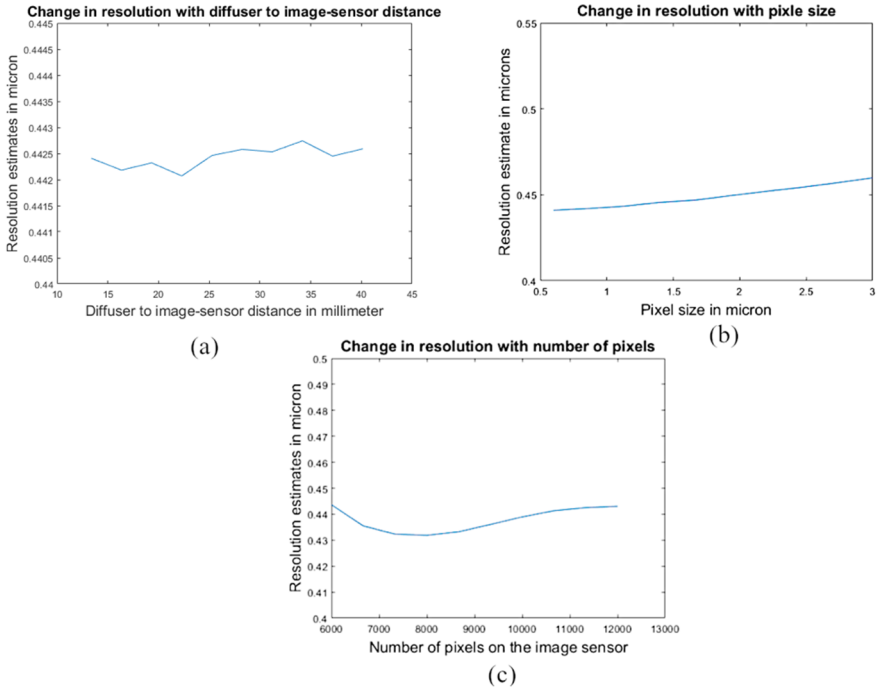


**Fig. 10.** Spatial resolution estimate of the lensless SRPE system (see Fig. 4) as a function of (a) distance from the diffuser to image sensor, (b) size of the pixels on the image sensor, and (c) number of pixels on the image sensor.

To analyze the effect of diffuser to sensor distance $z_2$ on the resolution estimate, we varied $z_2$ from 13.4 millimeters to 40.1 millimeters in steps of 2.6 millimeters. All the other system parameters were kept fixed at their initial values. Figure 10(a) shows that this causes only a 0.15% change in the resolution estimate (which is statistically insignificant), making this lensless SRPE system robust to changes in the diffuser to image-sensor distance. Also, the fluctuations in Fig. 10(a) are very small. Though Eq. (8) indicates that the maximum frequency collected by the sensor decreases with an increase in $z_2$, the random redistribution of the incoming frequency content performed by the diffuser ensures that high frequencies coming from the object are preserved even for a large $z_2$.

Sensor size is a product of two independent variables: pixel size $(p_\alpha, p_\beta)$, and the number of pixels $(M, N)$. In order to assess the effect of the pixel-size of the sensor, we have set $(M, N)$ fixed at $(2500, 2500)$ pixels, kept all the other system parameters fixed at their initial values, and varied the pixel size $(p_\alpha, p_\beta)$ from 0.6 microns to 3.0 microns in steps of 0.24 microns. Figure 10(b) shows that this causes the resolution estimate to increase from 0.4 microns to 0.46 microns, i.e., a 4.3% increase. To assess how the number of sensor-pixels affects resolution, we kept all the other system parameters fixed at their initial values and varied the number of pixels $(M, N)$ from $(6251, 6251)$ to $(12501, 12501)$. As shown in Fig. 10(c), this caused the resolution estimate to exhibit an overall change of 2.7%. Also, the fluctuations in Fig. 10(c) are very small. This study shows that within the aforementioned ranges, resolution estimates of single random phase encoded lensless imaging systems are robust to both the sensor pixel size and the number of pixels on the image sensor.

Optics EXPRESS

## 4. Conclusion

In conclusion, we have performed an analysis of the lensless single random phase encoding (SRPE) imaging system (see Fig. 4) to investigate its lateral resolution and robustness to some critical system parameters. We have used the angular spectrum method to propagate the field from two point-sources at the object plane of the imaging system through a diffuser and to the plane of the image sensor. This analysis establishes a baseline for the performance of a lensless SRPE imaging system. Since the angular spectrum method does not provide closed-form solutions for the SRPE system, we have used numerical simulations to finalize the analysis. This lateral resolution analysis provides a concrete relation between the physical parameters of the system and lateral resolution. Through our analysis and for the system parameters considered here, we have found that the lateral resolution of the lensless SRPE imaging system can be much smaller than the sensor pixel size. We have also compared this resolution estimate with that of a lens-based imaging system with similar system parameters. We found that lensless SRPE system offers resolution on par with lens-based systems even for lenses with high NA. However, lensless SRPE systems are more robust to many physical parameters of the system such as the pixel size and the number of pixels of the image sensor. Although the simulations are accurate up to the assumptions of angular spectrum propagation, the results are tethered to the thin diffuser model used for this analysis. However, real diffusers are much more complex. In the future, we shall perform analysis and experiments to verify the validity of the diffuser model used in this paper and provide a more accurate estimate of the spatial resolution.

## Appendix A

We list all the parameters defined in the paper in Table 2.

Optics EXPRESS

**Table 2. Definition of the parameters used in this paper**

| Parameters | Definition | Parameters | Definition |
|---|---|---|---|
| $\lambda$ | Wavelength of laser | $(x, y)$ | Co-ordinates of the object plane |
| $z_1$ | Distance from the object plane to the diffuser plane | $(\zeta, \eta)$ | Co-ordinates of the diffuser plane |
| $z_2$ | Distance from the diffuser plane to the image plane | $(\alpha, \beta)$ | Co-ordinates of the image sensor plane |
| $(f_{xm}, f_{ym})$ | Spatial frequencies corresponding to the object plane | $(f_{\zeta m}, f_{\eta m})$ | Spatial frequencies corresponding to the diffuser plane |
| $(\theta_{xm}, \theta_{ym})$ | Angles of the marginal ray leaving the object plane | $(\theta_{\zeta m}, \theta_{\eta m})$ | Angles of the marginal ray leaving the diffuser plane |
| $h_D(x, y)$ | Frequency filtering due to the aperture size of the diffuser | $h_S(\zeta, \eta)$ | Frequency filtering due to the aperture size of the image sensor |
| $(D_\zeta, D_\eta)$ | Spatial dimensions of the diffuser | $x_0$ | Separation between the two point-apertures placed on the object plane |
| $(p_\alpha, p_\beta)$ | Pixel size of the image sensor | $(S_\alpha, S_\beta)$ | Spatial size of the image sensor |
| $(pix_\alpha, pix_\beta)$ | Pixel pitch of the image sensor | $t_D(\zeta, \eta)$ | The transmittance function of the diffuser |
| $S(\cdot)$ | Sampling function of the image sensor | $P_A$ | Summation of the sampling function over the entire area of a pixel |
| $\mathcal{F}[\cdot]$ | Fourier transform | $\bar{N}$ | Number of source separations considered for the numerical simulation |
| $x_{0j}$ | Value of the $j$-th separation for numerical simulation | $(m, n)$ | Indices of pixels along horizontal and vertical directions |
| $x_{0j*}$ | The resolution estimate obtained through numerical simulation | $i_{Sj}$ | The sampled intensity corresponding to the $j$-th value of the source separation |
| $(M+1, N+1)$ | Number of pixels on the image sensor | $Corr(\cdot, \cdot)$ | Correlation metric for comparing intensities. Here, Frobenius norm. |
| SRPE | Single Random Phase Encoding | $th_{Corr}$ | Threshold value of $Corr(\cdot, \cdot)$ corresponding to the resolution estimate. |
| $u_0(x, y)$ | The input field | $u_1(x, y)$ | The complex field entering the diffuser |
| $u_2(\alpha, \beta)$ | The complex field incident on the image sensor plane | $i(\alpha, \beta)$ | The intensity of the field incident on the image sensor |
| $i_S[m, n]$ | The intensity sampled by the image sensor at pixel location $[m, n]$ | $f_l$ | The focal length of the lens-based imaging system equivalent to the SRPE lensless system under study. |

**Funding.** National Science Foundation (2141473); Office of Naval Research (N000142212375); Air Force Research Laboratory, Materials and Manufacturing Directorate (AFRL/RXMS) (FA8650-21-C-5711).

**Acknowledgments.** Distribution A. Approved for public release: distribution unlimited. (AFRL-2022-6020). Date approved 12-22-2022. The authors are grateful to Timothy O' Connor for all the valuable discussions and suggestions. We are also grateful to the anonymous reviewers for detailed remarks and careful reading of our manuscript which have substantially improved the quality of the manuscript.

**Disclosures.** The authors declare no conflicts of interest.

**Data availability.** No data were generated or analyzed in the presented research.

Optics EXPRESS

## References


1. B. Javidi, S. Rawat, S. Komatsu, and A. Markman, "Cell identification using single beam lensless imaging with pseudo-random phase encoding," Opt. Lett. **41**(15), 3663–3666 (2016).
2. B. Javidi, A. Markman, and S. Rawat, "Automatic multicell identification using a compact lensless single and double random phase encoding system," Appl. Opt. **57**(7), B190–B196 (2018).
3. A. Stern and B. Javidi, "Random Projections Imaging With Extended Space-Bandwidth Product," J. Display Technol. **3**(3), 315–320 (2007).
4. R. Corman, W. Boutu, A. Campalans, P. Radicella, J. Duarte, M. Kholodtsova, L. Bally-Cuif, N. Dray, F. Harms, G. Dovillaire, S. Bucourt, and H. Merdji, "Lensless microscopy platform for single cell and tissue visualization," Biomed. Opt. Express **11**(5), 2806–2817 (2020).
5. T. O'Connor, C. Hawxhurst, L. M. Shor, and B. Javidi, "Red blood cell classification in lensless single random phase encoding using convolutional neural networks," Opt. Express **28**(22), 33504–33515 (2020).
6. N. Antipa, G. Kuo, R. Heckel, B. Mildenhall, E. Bostan, R. Ng, and L. Waller, "DiffuserCam: lensless single-exposure 3D imaging," Optica **5**(1), 1–9 (2018).
7. P. M. Douglass, T. O'Connor, and B. Javidi, "Automated sickle cell disease identification in human red blood cells using a lensless single random phase encoding biosensor and convolutional neural networks," Opt. Express **30**(20), 35965–35977 (2022).
8. M. Martínez-Corral and G. Saavedra, "The resolution challenge in 3D optical microscopy," Prog. Opt. **53**, 1–67 (2009).
9. M. Born and E. Wolf, *Principles of Optics: Electromagnetic Theory of Propagation, Interference and Diffraction of Light*, 7th ed. (Cambridge University Press, 1999).
10. C. M. Sparrow, "On Spectroscopic Resolving Power," Astrophys. J. **44**, 76 (1916).
11. J. W. Goodman, *Introduction to Fourier optics*, 3rd ed. (Roberts and Company Publishers, 2005).